Numerical study of quantum vortex phase diagram in two-dimensional superconductors

Kiyokazu Myojin and Ryusuke Ikeda
Department of Physics, Kyoto University, Kyoto 606-8502, Japan

Shigeru Koikegami
Nanoelectronics Research Institute, AIST Tsukuba Central 2, Tsukuba 305-8568, Japan

(Received 6 February 2008; revised manuscript received 13 June 2008; published 11 July 2008)

Vortex phase diagrams of *weakly* disordered two-dimensional (2D) superconductors under a magnetic field perpendicular to the plane are numerically studied based on a recent development on the corresponding issue in three-dimensional (3D) systems with a low density of columnar defects at high temperatures. By examining the field dependences of magnetic quantities and the glass correlation, *two consecutive* first-order transitions (FOTs) are found to occur in weakly disordered cases even at low but finite temperatures, and the lower FOT is identified with a remnant of the melting transition of Bragg-Bose glass at zero temperature. The resulting phase diagram is discussed in relation to a FOT-like behavior found in superconducting thin films.

DOI: 10.1103/PhysRevB.78.014508 PACS number(s): 74.25.Dw, 74.40.+k, 74.78.−w, 74.20.De

I. INTRODUCTION

Vortex states of layered type-II superconductors in magnetic fields normal to each layer have been studied extensively so far in relation to phenomena in optimally doped high-T_c cuprates. Nevertheless, our understanding of the so-called vortex phase diagram still seems to be far from complete. In the case of a three-dimensional (3D) superconductor with just a weak point disorder but with no extended defects, the ordered phase in low fields and at low temperatures is believed to be the Bragg glass (BrG) (Refs. 1 and 2) (or an elastic glass[3]) with a quasi-long-ranged positional order of vortices. The counterpart[4] of BrG in the case with only line (or columnar) defects (LDs) parallel to the field and perpendicular to the layers has not been deeply discussed because, broadly speaking, LDs are believed to destroy a positional order of vortices due to their much stronger effect than weak point defects inevitably existing in real materials. In addition to this, the superconducting (SC) transition in systems with a large amount of LDs has been usually observed as a *continuous* transition. Through an analogy to the context of a quantum two-dimensional (2D) Bose system in a random environment, the resulting SC or glass phase is called Bose glass (BoG).[5] However, recent experiments in high-T_c cuprates with LDs have shown the presence of some first-order transition (FOT).[6–9] The observed FOT in bismuth strontium calcium copper oxide (BSCCO) with a low density of LDs is likely the melting transition of BoG into a vortex liquid (VL) (Ref. 6) according to the absence of vortex positional order below the FOT. On the other hand, according to a recent magnetic measurement in yttrium barium cooper oxide (YBCO) with a low density of LDs,[7] there is an anomaly of magnetization deep in the SC phase, similar to the sign of the first-order BrG melting in the case with only point disorders, in the field range where the BoG melting is also a FOT. It is reasonable to identify the phase below these magnetic anomalies as Bragg-Bose glass (BrBoG),[4] which is the counterpart of BrG in the case with LDs. The possibility of two separate FOTs in the H-T phase diagram (see Fig. 1) had been speculated in a previous theoretical work.[10] Further numerical simulations for layered systems have also shown the presence of double FOTs accompanied by a BrG-like low-temperature phase.[11,12] Hereafter, we call such a layered system at high temperatures with LDs as the thermal 3D case.

A closely related issue to the thermal 3D case mentioned above is that of disordered thin films in a field perpendicular to the plane in the *quantum* regime near zero temperature. In this quantum 2D case, the model corresponding to the Ginzburg-Landau (GL) Hamiltonian $\mathcal{H}[\Psi]$ for the thermally fluctuating SC order parameter Ψ is a quantum Euclidean *action* $\mathcal{S}[\Psi(\tau)]$ represented in the space-(imaginary)time, in which the fluctuating SC order parameter $\Psi(\tau)$ is a dynamical quantity and depends on the imaginary time τ. Hence, the pointlike *static* disorder in the film plays, in $\mathcal{S}$, the roles of a correlated disorder persistent in the τ direction taken perpendicular to the film plane. Then, the problem of the 2D phase diagram in the present case is, in the low-temperature limit, similar to that of the thermal 3D case. In addition, studies of the 2D vortex phase diagram at finite temperatures will also play a role in understanding finite-size effects in the thermal 3D case.

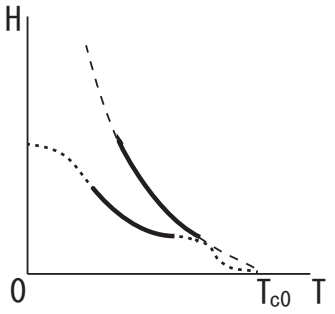

FIG. 1. One of expected H-T phase diagrams in the thermal 3D case with a low density of LDs (Ref. 10), which, generically, has a lower critical point (Refs. 9, 10, and 13) of the higher FOT line. The solid and dashed curves denote FOTs and second-order glass transitions, respectively. The portion of the dotted line of the lower FOT has not been detected yet experimentally (Ref. 7). Alternatively, the two FOT lines may merge with each other if the disorder is weak enough (Ref. 10).

A scaling behavior seen in resistivity data in thin SC films has been discussed so far in several materials as evidence of a magnetic field–tuned superconductor-insulator (FSI) quantum *continuous* transition.[14,15] It is believed that a FSI quantum transition suggested by the resistive data is a second-order (vortex) glass transition[16] in disordered 2D superconductors at zero temperature ($T=0$) corresponding to the BoG to VL transition in the thermal 3D case with a *high* density of LDs. Then, based on the similarity to the thermal 3D case mentioned above, it is natural to expect the presence of some FOT in films with a *low* density of LDs at least in the low-T limit. In fact, resistivity measurements in amorphous MoGe films with a relatively low sheet resistance have shown a nearly discontinuous vanishing of resistance at fields much lower than the apparent FSI transition field.[15] Among the SC films[14,15,17] showing a resistive behavior suggestive of a FSI quantum transition, MoGe has a remarkably weak pinning effect.[18] If we can understand why another FOT, corresponding to the BoG melting transition in the thermal 3D case mentioned above, is easily changed into a continuous FSI transition in this 2D quantum case, it is natural to identify the observed FOT-like behavior[15] as the counterpart of the BrBoG melting occurring in the thermal 3D case with a low density of LDs.

Motivated by such a connection between the quantum 2D and the thermal 3D vortex systems, we numerically examine the vortex phase diagram in a layered quasi-2D superconductor under a field **H** perpendicular to the layers and with LDs parallel to **H** by changing the number of layers or the strengths of randomness and fluctuation. We use the GL action expressed in terms of the SC order parameter $\Psi(\tau)$ in the lowest Landau level (LLL) in the type-II limit where the magnetic screening is negligible. Taking the type-II limit is rather appropriate to the 2D quantum case in which the magnetic penetration depth $[\lambda(0)]^2/D_t$ is often longer than the sample size, where $\lambda(0)$ is the London penetration depth and D_t is the film thickness.[19] It is numerically found that, in general, two FOTs may occur in the quantum 2D regime. The FOT at a higher field can be identified as a BoG transition, while the lower one is presumably the BrBoG melting. However, as the number of layers diminishes and/or the randomness is stronger, the higher FOT tends to disappear more easily than the lower one does. The resulting numerical data are discussed in relation to closely related experimental results.[7,15] The present results imply that at lower temperatures than those seen experimentally, one or two FOTs might be present even in the SC thin films, suggesting the presence of a second-order FSI transition. The presence of two FOTs in the thermal 3D case has been preliminarily reported elsewhere.[12]

This paper is organized as follows: In Sec. II, we describe the GL action used in this work and explain the correspondence between the quantum 2D and the thermal 3D cases. In Sec. III, we present our simulation results. In Sec. IV, quantum 2D phase diagrams that we propose based on our results are shown and discussed. The unit $\hbar=c=k_B=1$ will be used below.

II. MODEL AND PHYSICAL QUANTITIES

To construct a model useful in numerical simulations, let us first start from the familiar quasi-2D GL Hamiltonian in an external magnetic field **H** perpendicular to the layers,

$$\mathcal{H}[\Psi] = \mathcal{H}_0 + \mathcal{H}_p, \tag{1}$$

where

$$\mathcal{H}_0 = \sum_{j=1}^{N_L} \int d^2\mathbf{r}_\perp \left[\Psi_j^* \alpha(\Pi^2)\Psi_j + \gamma|\Psi_{j+1}(\mathbf{r}_\perp) - \Psi_j(\mathbf{r}_\perp)|^2 + \frac{\beta}{2}|\Psi_j(\mathbf{r}_\perp)|^4 \right], \tag{2}$$

$$\mathcal{H}_p = \sum_{j=1}^{N_L} \int d^2\mathbf{r}_\perp u(\mathbf{r}_\perp)|\Psi_j(\mathbf{r}_\perp)|^2. \tag{3}$$

Throughout this paper, the length scales within the layers are assumed to have been normalized by the in-plane coherence length ξ_0. In $\mathcal{H}_0$ and $\mathcal{H}_p$, $\Psi_j(\mathbf{r})$ is the SC order parameter defined on the jth layer, $\boldsymbol{\Pi} \equiv -i\nabla + 2|e|\xi_0\mathbf{A}$ denotes the gauge-invariant gradient defined along the layers, curl $\mathbf{A} = H\xi_0\hat{z}$, N_L is the number of layers, and the interlayer-coupling constant $\gamma(>0)$, as well as α, is a dimensionless parameter. Further, irrespective of the dimensionality of the system, $\beta(>0)$ is the main parameter determining the fluctuation strength because it is inversely proportional to both of the interlayer spacing D_t and the magnitude of the condensation energy. Note that the random potential $u(\mathbf{r}_\perp)$ is independent of j, implying a static disorder *correlated* along **H** perpendicular to the layers, and that the magnetic energy term is absent in Eq. (1) because we invoke the type-II limit. Since we focus on Ψ in LLL, Π^2 in α may be replaced by $2|e|\xi_0^2 H \equiv l^{-2}$. Then, the mean field H_{c2} is the field value at which $\alpha=0$, and α increases with increasing H. The potential $u(\mathbf{r})$ satisfies

$$\overline{u(\mathbf{r})} = 0,$$

$$\overline{u(\mathbf{r})u(\mathbf{r}')} = p\,\delta(\mathbf{r}-\mathbf{r}'),$$

where the overbar implies the random average. That is, the pinning strength is measured in our model just by the parameter p proportional to the defect density. The partition function is given by

$$\mathcal{Z} = \mathrm{Tr}_\Psi \exp(-\mathcal{H}/k_BT) \tag{4}$$

in the thermal quasi-2D (3D) case. Following previous works,[20,21] $\Psi_j(\mathbf{r})$ satisfies the semiperiodic boundary condition within the jth layer,

$$\Psi_j(x, y+L_y) = \Psi_j(x,y),$$

$$\Psi_j(x+L_x, y) = \Psi_j(x,y)\exp\left(i\frac{2\pi N_s}{L_y}y\right).$$

In addition, the periodic boundary condition

$$\Psi_{j+N_L}(x,y) = \Psi_j(x,y).$$

will be assumed in the direction parallel to **H**. Further, $\Psi_j(\mathbf{r})$ is expanded in terms of the LLL eigenfunction

$$\varphi_n(\mathbf{r}) = \left(\frac{1}{\sqrt{\pi}L_y l}\right)^{1/2} \sum_{N=-\infty}^{\infty} \exp\left[-\frac{1}{2l^2}(x - X_{n,N})^2\right] \exp\left(\mathrm{i}X_{n,N}\frac{y}{l^2}\right)$$

as

$$\Psi_j(\mathbf{r}) = \sum_{n=0}^{N_s-1} c_{n,j}\varphi_n(\mathbf{r}), \tag{5}$$

where n is the integer which satisfies $0 \leq n \leq N_s - 1$, N is an arbitrary integer,

$$X_{n,N} = X_n + L_x N = \frac{2\pi l^2}{L_y} n + L_x N,$$

$X_n \equiv X_{n,N=0}$, and $N_s = N_x N_y$ is the number of vortices. The system size in each direction is $L_\mu i\mu = xCyj$, which satisfies the relations[20,21] $L_x L_y = 2\pi l^2 N_s$ and $L_x/L_y = \sqrt{3}N_x/2N_y$. The quartic term will be expressed as

$$\int d^2\mathbf{r}|\Psi_j(\mathbf{r})|^4 = \frac{1}{L_x L_y}\sum_{\mathbf{k}} |\Delta_j(\mathbf{k})|^2,$$

where $\Delta_j(\mathbf{k})$ is the Fourier transformation of $|\Psi_j(\mathbf{r})|^2$,

$$\begin{aligned}\Delta_j(\mathbf{k}) &= \int d^2\mathbf{r}|\Psi_j(\mathbf{r})|^2 \exp\left(-i\frac{\mathbf{k}\cdot\mathbf{r}}{l}\right) \\ &= \sum_N \sum_{n_1,n_2} c_{n_1,j}c^*_{n_2,j}\delta_{n_1-n_2+N_sN,\ m_y} \\ &\quad \times \exp\left(-\frac{k^2}{4}\right)\exp\left(-i\frac{X_{n_1}+X_{n_2}+L_xN}{2l}k_x\right).\end{aligned} \tag{6}$$

$\delta_{\mu,\nu}$ denotes the Kronecker delta, and $k_\mu = 2\pi l m_\mu / L_\mu$, with an integer $m_\mu (\mu = x, y)$. Using these expressions, $\mathcal{H}_0$ is written in LLL as[21]

$$\begin{aligned}\mathcal{H}_0 = \sum_{n,j}\Bigg[&\alpha(l^{-2})|c_{n,j}|^2 + \gamma|c_{n,j+1} - c_{n,j}|^2 + \frac{\beta}{2\sqrt{2\pi}lL_y} \\ &\times \sum_{n_1,n_2,n_3}\sum_{N_1,N_2} c^*_{n_1,j}c^*_{n_3,j}c_{n,j}c_{n_2,j}\delta_{n_1+n_3+N_s(N_1+N_2),n_2+n} \\ &\times \exp\Bigg\{-\frac{\sqrt{3}\pi}{2N_y^2}[(n_1 - n_2 + N_sN_1)^2 + (n_3 - n_2 \\ &+ N_sN_2)^2]\Bigg\}\Bigg].\end{aligned} \tag{7}$$

Below, the LLL approach for the thermal 3D or quasi-2D case, illustrated above, will be extended to the corresponding 2D quantum action as a model for studying the phase diagram of thin films at low temperatures. Before performing this, however, we need to explain how the ordinary GL model, Eq. (1), used conventionally near T_c is qualitatively applicable to studies in the quantum regime. In higher fields and lower temperatures, not only α but also all coefficients appearing in the GL Hamiltonian are operators including Π^2 and dependent on the underlying electronic model. In LLL, however, they can be expressed as coefficients dependent on l. Hence, the LLL approach can be extended to such higher fields by including field and temperature dependences of *microscopic* origins in each coefficient of the GL Hamiltonian.[22,23] In addition, the main role of such microscopic l dependences is, just like the l dependence of α in Eq. (1), to increase the magnitude of the condensation energy with decreasing l^{-2}. Thus, in order to obtain a *qualitatively* valid l dependence of the condensation energy, we only have to keep the l dependence of only α as far as other coefficients such as β and γ in Eq. (1) show no sign change upon sweeping the field. Actually, our main purpose in the present work is to show the presence of FOTs which occur in narrow field ranges, where the microscopic l dependences of the coefficients are clearly irrelevant.

Next, the applicability of the LLL approach in studies of phase transitions between different vortex phases will be discussed. This approach is conventionally used by neglecting possible fluctuations of the flux density and, hence, is valid for systems with a large enough GL parameter. In single crystals of YBCO, this approximation is safely valid in fields in the Tesla range,[10] while it is not useful in BSCCO in fields less than 100 G, where vortex lattice melting is found to occur and a *magnetic* interlayer coupling between pancake vortices is important.[24] On the other hand, as already mentioned in Sec. I, the approximation of the type-II limit is safely valid in 2D systems. Further, the LLL approach was useful, in clean limit, in obtaining reasonable generic phase diagrams both in 2D (Refs. 20 and 25) and quasi-2D (Ref. 26) cases, in which a single FOT occurs between VL and the Abrikosov lattice. In the case with quenched disorder, in contrast, extensive studies of the vortex phase diagram in LLL seem to have been limited so far to the 2D case, where, as expected, no clear sign of a transition was found at finite temperatures.[27] On this background, it will be valuable to clarify whether a quasi-ordered state such as BrG and BrBoG is realized within the LLL approach for quasi-2D systems composed of multilayers. In addition to this, a reasonable description of the FSI transition in the quantum regime was also developed in the LLL approach.[23] For these reasons, we believe that at the qualitative level, the LLL approach based on the GL model is convenient and useful in studying the vortex phase diagrams comprehensively.

Now, let us turn to giving a quantum 2D GL *action* equivalent to the Hamiltonian in Eq. (1). Such a GL action can be found for a quantum Josephson-junction array with a charging energy term and a randomness of the Josephson-coupling energy, which is a standard model of a disordered granular superconductor. If we focus on a relatively low magnetic field range in which the disorder-induced *phase glass* ordering is negligible, the quenched disorder is treated as the potential disorder of the type represented by $\mathcal{H}_p$ in Eq. (1).[28] Further, if the Ohmic dissipation is negligible and the intragrain contribution to the charging energy dominates over the corresponding intergrain one, the effective action of the quantum 2D Josephson-junction array can be expressed by[28]

$$\begin{aligned}\tilde{\mathcal{S}}_Q[\Psi(\tau)] = \int d^2\mathbf{r}\int_0^{T^{-1}} d\tau\Bigg[&\gamma_{\mathrm{nd}}|\partial_\tau\Psi(\mathbf{r},\tau)|^2 + [\alpha(l^{-2}) + u(\mathbf{r})] \\ &\times|\Psi(\mathbf{r},\tau)|^2 + \frac{\beta}{2}|\Psi(\mathbf{r},\tau)|^4\Bigg],\end{aligned} \tag{8}$$

which is of the same form as the continuum limit of Eq. (1)

if the coordinate jD_t perpendicular to the layers in model (1) is identified with the imaginary time τ. Corresponding to Eq. (8), the partition function is given by

$$\mathcal{Z} = \mathrm{Tr}_{\Psi} \exp(-\tilde{\mathcal{S}}_Q). \tag{9}$$

In Secs. III and IV, we present results of numerical simulations for the nondissipative model [Eq. (8)] and will discuss experimental observations in nominally amorphouslike thin films.[15]

However, Eq. (8) is not directly applicable to amorphouslike superconductors because the quantum dynamical term of the corresponding effective GL action is dominated in such systems by the dissipative one: According to the standard functional-integral technique,[29] the following GL action or functional can be derived based on an electronic Hamiltonian with an attractive interaction term of BCS type:[29]

$$\mathcal{S}_Q = \int d^2\mathbf{r}\left\{ T\sum_{\omega} \gamma_{\mathrm{d}}|\omega||\Psi_{\omega}(\mathbf{r})|^2 + \int_0^{T^{-1}} d\tau\left[[\alpha(l^{-2}) + u(\mathbf{r})] \times|\Psi(\mathbf{r},\tau)|^2 + \frac{\beta}{2}|\Psi(\mathbf{r},\tau)|^4 \right]\right\}, \tag{10}$$

where $\Psi(\mathbf{r},\tau) = T\Sigma_{\omega}\Psi_{\omega}(\mathbf{r})\exp(-\mathrm{i}\omega\tau)$, $\gamma_{\mathrm{d}} \geq 0$, and ω is the bosonic Matsubara frequency. As mentioned earlier, γ_{d} as well as other coefficients depends on l at low temperatures. Note the difference in the dynamical term between Eqs. (8) and (10). This should be reflected in the difference of the universal class of the quantum critical behavior of the second-order BoG transition at $T=0$. As far as focusing on the presence or absence of FOTs in the quantum regime by neglecting the *details* of the quantum *critical* fluctuation mentioned above, however, our study of the nondissipative model, Eq. (8), is also useful in judging expected phase diagrams in the purely dissipative case. In fact, it will be explained in Sec. IV that the main features, closely related to the experimental observation,[15] of the vortex phase diagram following numerically from the nondissipative model, Eq. (8), should be found in the corresponding results of the dissipative model.

To make action (8) tractable numerically, the continuous imaginary time variable will be discretized in the manner $\tau \rightarrow j\Delta_{\tau}$, and the τ integral in Eq. (8) will be replaced by a summation. After rescaling $\Delta_{\tau}^{1/2}\Psi_j \rightarrow \Psi_j$, the resulting GL action takes the following form:

$$\mathcal{S} = \int d^2\mathbf{r}_{\perp} \sum_{j=0}^{N_L-1} \left[\bar{\gamma}|\Psi_j(\mathbf{r}_{\perp}) - \Psi_{j+1}(\mathbf{r}_{\perp})|^2 + [\alpha(l^{-2}) + u(\mathbf{r}_{\perp})] \times|\Psi_j(\mathbf{r}_{\perp})|^2 + \frac{\bar{\beta}}{2}|\Psi_j(\mathbf{r}_{\perp})|^4 \right], \tag{11}$$

where $\Psi_j(\mathbf{r}_{\perp}) = \Psi(\mathbf{r}_{\perp}, j\Delta_{\tau})$, and

$$\bar{\beta} = \frac{\beta}{\Delta_{\tau}},$$

$$\bar{\gamma} = \frac{\gamma_{\mathrm{nd}}}{\Delta_{\tau}^2} \tag{12}$$

are dimensionless quantities. It is reasonable to, just like the interlayer spacing D_t in the thermal quasi-2D model [Eq. (1)], fix the thickness of each time slice $\Delta_{\tau} = (TN_L)^{-1}$ to a time scale of $\mathrm{O}(T_{c0}^{-1})$, where T_{c0} is the mean-field SC transition temperature in $H=0$. In fact, in searching for a transition in 3D systems using a quasi-2D model with a finite D_t, it is often unnecessary to take the $D_t \rightarrow 0$ limit. Thus, by choosing Δ_{τ} to be a fixed value of $\mathrm{O}(T_{c0}^{-1})$, the temperature T will be measured under model (11) by N_L in the manner

$$T = \frac{1}{N_L\Delta_{\tau}} \propto N_L^{-1}, \tag{13}$$

while the applied field H is primarily measured by α. By noting that Eq. (11) is of the same form as $\mathcal{H}/T$ given in Eq. (1), the action obtained by rewriting Eq. (11) in the form of Eq. (7) will be used hereafter as a model for numerical simulations in *both* the quantum 2D and the thermal 3D cases.

Since we focus on the low-temperature regime in the quantum 2D case, the *microscopic* T dependences of the coefficients α, $\bar{\beta}$, and $\bar{\gamma}$ are cut off[22] by the finite l^{-2} and, hence, may be neglected. Hereafter, we will assume the relation $\alpha = l^{-2} - 1 = [H/H_{c2}(0)] - 1$. Further, $\bar{\beta}$ will be estimated as follows: Using the well-known relation between $\bar{\beta}$ and the London penetration depth $\lambda(0)$, we have the relation $\bar{\beta} = 32\pi[e\lambda(0)]^2/(D_t\Delta_{\tau})$. For simplicity, we set $\Delta_{\tau} = T_{c0}^{-1}$. Then, for the parameter values $\lambda(0) = 10^3$ (A), $T_{c0} = 1$ (K), and $D_t = 10$ (A), we have $\bar{\beta} = 3 \times 10^{-3}$. Below, $\bar{\beta}$ values comparable with this estimate will be used.

In our numerical simulation to be explained in Sec. III, the H dependences of physical quantities are investigated at a fixed temperature. By noting that the number of vortices N_s is proportional to H under fixed L_x and L_y (system sizes), two kinds of simulations have been performed in this research. One is a simulation under a fixed N_s, and the other is based on the use of fixed L_x and L_y.[12] We have found that the former simulation in which L_{μ}/l $(\mu = x, y)$ is fixed in changing H gives much clearer results. Hereafter, we will present just the simulation results obtained under the *fixed* number of vortices $N_s = 64$. Based on previous works in LLL in the thermal 2D case,[20,27] simulations with $N_s = 64$ are expected to give essentially correct results on the phase diagram.[20,21]

The physical quantities we examine in the quantum 2D case will be defined below. In the present system, a FOT is observed as a jump and some hysteresis of the internal energy or the magnetization. In a GL functional derived microscopically, the magnetization M is given as an appropriate sum of the ensemble and spatial averages of $|\Psi_j|^2$, $|\Psi_j|^4$, and other higher-order GL terms because the coefficients of all terms of the GL functional $\mathcal{S}$ are H dependent in general. On the other hand, if only the H dependence of α is taken into account in Eq. (11), $-M$ is equivalent to the average of the $|\Psi_j|^2$ term, and then, in the quantum 2D case, we may have to measure only a hysteresis of the $|\Psi_j|^2$ term upon sweeping. Since the so-called Abrikosov factor measuring the

structure of the vortex state is proportional to the average of the $|\Psi_j|^4$ term in $\mathcal{S}$, the $|\Psi_j|^4$ term should also show a hysteresis at a FOT between different vortex states. That is, any summation of the spatial average of the $|\Psi_j|^2$ term and that of the $|\Psi_j|^4$ one can become a measure of a hysteresis due to a FOT. On the other hand, in the thermal 3D case, we should examine a hysteresis of the Hamiltonian itself given in Eq. (1).[20] Below, we choose to examine the following quantity proportional to the hysteresis of $\mathcal{S}$ upon sweeping the magnetic field:

$$\Delta E = \frac{1}{2\pi N_s N_L}[\overline{\langle \mathcal{S} \rangle_{\mathrm{dec}}} - \overline{\langle \mathcal{S} \rangle_{\mathrm{inc}}}], \tag{14}$$

where the index "inc" ("dec") denotes the process increasing (decreasing) H. For the initial condition of Ψ, we employ the mean-field solution of the triangular vortex lattice in the process increasing H (i.e., l^{-1}), while the vanishing Ψ is initially used for the process decreasing H.

Next, to observe a configuration of vortices at each H, we have examined the structure factor

$$I(\mathbf{k}) \equiv \overline{\left\langle \frac{N_L \sum_j |\Delta_j(\mathbf{k})|^2}{\left[\sum_j \Delta_j(0)\right]^2} \right\rangle}, \tag{15}$$

where $\Delta_j(\mathbf{k})$ is given by Eq. (6). The magnetization M of model (11) may be defined as

$$M = -N_L^{-1} \sum_j \int d^2\mathbf{r} \overline{\langle |\Psi_j(\mathbf{r})|^2 \rangle} = -N_L^{-1} \sum_{n,j} \overline{\langle |c_{n,j}|^2 \rangle}, \tag{16}$$

where a H dependent coefficient was set to be unity. Since M in the quantum 2D case, as well as the entropy in the thermal 3D case, is a first derivative of the free energy and may not necessarily reflect the details of a higher-order transition or a sharp crossover, we have preferred calculation of the following differential susceptibility:

$$\chi \simeq \frac{\partial}{\partial \alpha} M = \frac{1}{N_L} \sum_{n,j} \sum_{n',j'} [\overline{\langle |c_{n,j}|^2 |c_{n',j'}|^2 \rangle} - \overline{\langle |c_{n,j}|^2 \rangle \langle |c_{n',j'}|^2 \rangle}], \tag{17}$$

which, in the thermal 3D case, corresponds to the heat capacity normalized by its mean-field jump value in $H=0$ at T_c. This quantity helps us to distinguish a genuine transition in the low-T ($N_L \to \infty$) limit from just a crossover. For the same purpose, we have also examined the glass correlation length ξ_G. To define ξ_G, we have employed the Fourier transform of the glass correlation function $\mathcal{G}_G$,[16,30]

$$\begin{aligned} \mathcal{G}_G(\mathbf{k}, k_z = 0) &= \frac{1}{L_x L_y N_L} \sum_{j,\tilde{j}} \int d^2\mathbf{r} \int d^2\tilde{\mathbf{r}} \overline{|\langle \Psi_j(\mathbf{r}) \Psi^*_{j+\tilde{j}}(\mathbf{r}+\tilde{\mathbf{r}}) \rangle|^2} \exp\left(-i \frac{\mathbf{k} \cdot \tilde{\mathbf{r}}}{l}\right) \\ &= \frac{1}{L_x L_y N_L} \sum_{j,\tilde{j}} \sum_{n_1,n_2} \sum_{N} \overline{\langle c_{n_1,j} c^*_{n_2,j+\tilde{j}} \rangle \langle c^*_{n_1+N_s N-m_y,j} c_{n_2+N_s N-m_y,j+\tilde{j}} \rangle} \exp\left(-\frac{k^2}{2}\right) \exp\left(-i \frac{X_{n_1} - X_{n_2}}{l} k_x\right), \end{aligned} \tag{18}$$

where $k_y = 2\pi l m_y / L_y$. Generally, ξ_G in the VL region is derived from

$$\xi_G^2 = -l^2 [\tilde{\mathcal{G}}_G(\mathbf{k})]^{-1} \left. \frac{\partial}{\partial k^2} \tilde{\mathcal{G}}_G(\mathbf{k}) \right|_{\mathbf{k}=0}$$

because the correlation function there is expressed as $\tilde{\mathcal{G}}_G \propto 1/(k^2 + l^2 \xi_G^{-2})$. Consequently, for simulations using a finite system size, we can write it down as

$$\xi_G = \frac{l}{2 \sin(k_{\min}/2)} \left[\frac{\tilde{\mathcal{G}}_G(0)}{\tilde{\mathcal{G}}_G(k_{\min})} - 1 \right]^{1/2}. \tag{19}$$

Although we set $k_{\min} = 2\pi l / L_y$, this expression can be defined as the correlation length because the system is essentially isotropic in the x-y plane.

III. NUMERICAL RESULT

We have performed Monte Carlo (MC) simulations of the model, Eq. (11), to detect FOTs into glass phases or regimes. We have used the parameter values $\bar{\gamma}=0.1$ and $N_x=N_y=8$ for all simulations and have examined the systems with one, two, four, and eight layers (i.e., $N_L=1$, 2, 4, and 8) in the pure ($p=0$) and disordered ($p=1.0\times10^{-4}$, 2.0×1.0^{-4}, and 3.0×10^{-4}) cases. The largest size we use, $N_x N_y N_L = 512$, is comparable with 560 in Ref. 26 and larger than those used in Ref. 21 The fluctuation strength has also been changed by choosing the values $\bar{\beta}=1.0\times10^{-2}$, 5.0×10^{-3}, and 2.0×10^{-3} [see the estimations given below Eq. (13)]. The Markov chains for $c_{n,j}$ were generated by the Metropolis algorithm. We have used the first $(2-4)\times10^5$ MC steps for thermalization, and additional 5.0×10^4 MC steps have been used for observation, in particular, of a FOT occurring deep in the glassy regime.

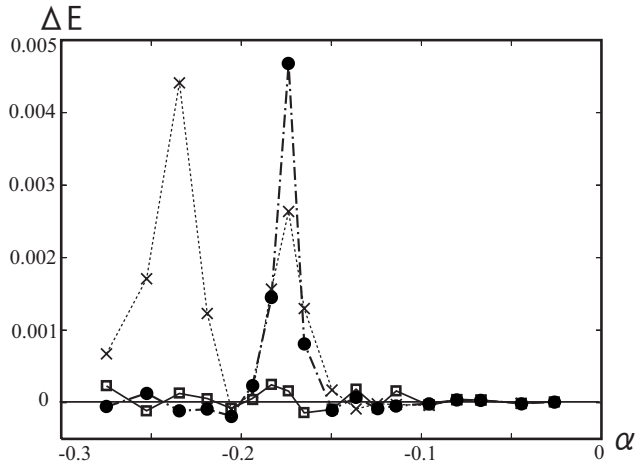

FIG. 2. ΔE data for different p values, $p=0$ (solid circles), 1.0×10^{-4} (crosses), and 3.0×10^{-4} (open squares), of the $N_L=4$ system for $\bar{\beta}=1.0\times10^{-2}$. For $p=0$, the low-field phase is a nearly perfect vortex lattice which occurs below a single FOT at $\alpha\simeq-0.17$. In contrast, in the case with $p=3.0\times10^{-4}$, no clear hysteresis appears anywhere, reflecting a second-order BoG to VL transition at $T=0$, which, in the large N_L limit, presumably occurs in $\alpha\geq-0.18$ (see Figs. 9 and 10). In the intermediate value $p=1.0\times10^{-4}$, we have two FOTs with remarkable hysteresis indicative of a BrBoG to BoG and a BoG to VL transition.

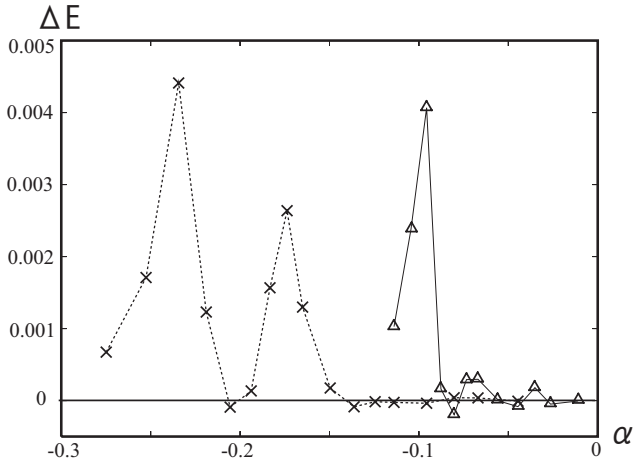

FIG. 3. ΔE data for $\bar{\beta}=2.0\times10^{-3}$ (open triangles) and 1.0×10^{-2} in the $N_L=4$ system with $p=1.0\times10^{-4}$. The result for $\bar{\beta}=1.0\times10^{-2}$ is the same as in Fig. 2.

We stress that our simulation is performed at finite T, i.e., for layered systems with a finite number of layers [see Eq. (13)]. Hence, strictly speaking, we address only the VL regime when the disorder is nonvanishing ($p>0$) because no glass phases are believed to be present in *disordered* 2D systems at finite T.[27] Nevertheless, as seen below, we find that FOTs, signaled by some hysteresis which survives even when MC steps are increased enough, appear only at low enough temperatures (i.e., for larger N_L values). That is, although no true glass phase is expected, FOTs survive at low but nonzero T. Such a situation is similar to the VL to vortex slush transition in the context of the thermal 3D case argued in Refs. 31 and 32 and verified numerically[33] and experimentally,[34] where the vortex liquid and slush states are continuously connected with each other because of the presence of a critical end point of a FOT. Below, the *regime* in fields lower than a detected FOT will be often called in this sense as BoG or BrBoG by assuming that our computations at finite T reflect the corresponding phase diagram in the $T\rightarrow0$ limit.

A. First-order transitions

Let us first start by explaining dependences on the disorder or the vortex-pinning strength of ΔE data. Examples of such data are shown in Fig. 2. In this and ensuing figures expressing ΔE vs α, a measurably large peak of ΔE in a narrow α (i.e., field) range implies some hysteresis accompanying a FOT. We have verified that each of such hysteresis survives even for more MC steps; hence, we argue that it is an intrinsic event accompanying a phase transition in equilibrium. Figure 2 shows the p dependences of ΔE in the $N_L=4$ case for three values of the pinning strength, $p=0$, 1.0×10^{-4}, and 3.0×10^{-4}. In the perfectly clean ($p=0$) case, no glass phases are present, and the only ordered *phase* is the vortex lattice occurring through a single FOT at $\alpha\simeq-0.17$ even at finite temperatures. In the weak disorder case with $p=1.0\times10^{-4}$, we find *two consecutive* FOTs upon sweeping the field. Based on the argument in Ref. 10, the low-field *regime* is expected to correspond to BrBoG,[35] while the BoG *regime* is expected to exist between the two FOTs in the low $T\propto N_L^{-1}$ limit. That is, the FOT in clean limit has split into two FOTs to induce BoG as an intermediate regime in the range $0<p<1.0\times10^{-4}$. Here, it is a remarkable feature that, as seen in experiments in high-T_c cuprates,[9,36] the position of the first-order BoG melting is almost the same as the FOT in clean limit (see Ref. 10). Finally, for the stronger disorder ($p=3.0\times10^{-4}$), both FOTs seen for $p=1.0\times10^{-4}$ have been lost. Based on the common view on the 3D system with a high density of LDs explained in Sec. I, this case corresponds, if realized even in large N_L limit, to a system at $T=0$ with a second-order BoG to VL transition but with no BrBoG. However, since there is no reason why the two FOTs should be lost altogether at the same p value, we expect the presence of a p range in which either of them survives.

To verify the presence of a situation with a single FOT for finite p values, we have investigated the dependences of those FOTs on the fluctuation strength $\bar{\beta}$ instead of trying to find their subtle p dependences in a narrow p range because a decrease in fluctuation at a fixed p would imply an effective enhancement of the vortex-pinning strength. As Fig. 3 shows, either of the two FOTs in $\bar{\beta}=1.0\times10^{-2}$ has disappeared when $\bar{\beta}=2.0\times10^{-3}$. However, since the position of the remaining transition has shifted to a remarkably higher field, it is not necessarily clear from this figure which of the FOTs has disappeared. To examine the positional ordering of vortices above and below the remaining FOT, the snapshots of the structure factor in $\bar{\beta}=2.0\times10^{-3}$ case are shown in Fig. 4. The sharp Bragg peaks in (a) showing a hexagonal symmetry suggest that when $\bar{\beta}=2.0\times10^{-3}$, the vortex state be-

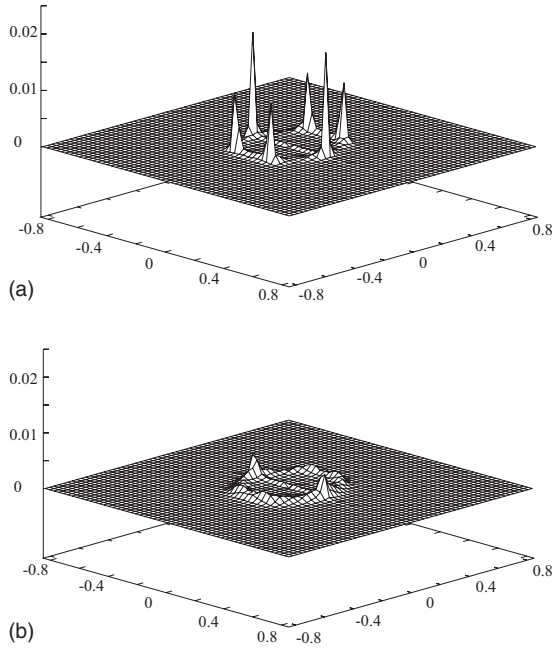

FIG. 4. Snapshots of the structure factor in the $\bar{\beta}=2.0\times10^{-3}$ case in Fig. 3 for (a) $\alpha=-0.12$ and (b) $\alpha=-0.07$. The vortex state *just* above the FOT corresponds to BoG.

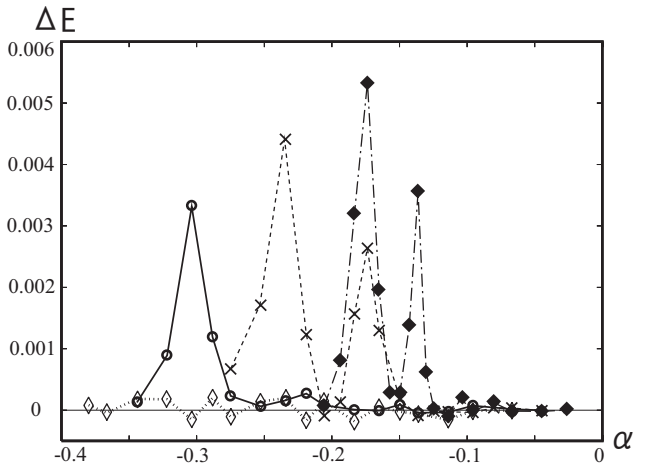

FIG. 5. ΔE data in systems with different N_L under the fixed parameters $p=1.0\times10^{-4}$ and $\bar{\beta}=1.0\times10^{-2}$. The data of the cases with $N_L=8$ (solid squares) and 4 (crosses) show hysteresis around *two* α values, while hysteresis in the $N_L=2$ system (open circles) occurs only around a single α value. In addition, in the $N_L=1$ case (open diamonds) corresponding to the purely thermal 2D case, no hysteresis implying a FOT is seen (Ref. 27). Both of the two hysteresis peaks seen in the $N_L\geq4$ shift to higher fields when $N_L=8$ (i.e., as temperature decreases).

low the remaining FOT is a nearly triangular vortex lattice. That is, it is expected that this FOT in $\bar{\beta}=2.0\times10^{-3}$ is the BrBoG to BoG transition, while the BoG melting transition has changed into a second-order one in large N_L limit. This conjecture[35] that the first-order melting transition of BrBoG is more robust than the first-order melting of BoG is also supported by the N_L dependence of the phase diagram given below.

Here, we note that in the structure factors following from our computations using $N_s=64$, a weak twofold anisotropy is seen in the x-y plane (see Fig. 4). This anisotropy is a consequence of the use of the finite N_s value and of the Landau gauge for the external vector potential $\mathbf{A}$. Of course, for a larger N_s value,[20] such a specific anisotropy is not seen in states with the triangular lattice symmetry. However, since this anisotropy for $N_s=64$ is seen even in high enough fields near H_{c2} and, hence, is merely a bystander in the phase diagram, it does not seem that this anisotropy induced by the small N_s has played an essential role in obtaining phase diagrams.

In Fig. 5, ΔE vs α curves computed in terms of $p=1.0\times10^{-4}$ and $\bar{\beta}=1.0\times10^{-2}$ are shown for $N_L=1$, 2, 4, and 8 systems. For the moment, we focus on the cases of $N_L=4$ and 8, in which two consecutive FOTs are seen. One finds that with decreasing $T\propto N_L^{-1}$, the transition points shift to higher fields, reflecting the T dependence of the vortex lattice melting field in the $p=0$ case, and that the BoG regime becomes narrower. Three snapshots of the structure factor in the $N_L=8$ case below the lower FOT, above the higher FOT, and in the intermediate fields are shown in Fig. 6. We believe that our identification based on these figures between the three regimes and the three vortex states in the $T\to0$ limit (BrBoG, BoG, and VL) is justified. Below the lower FOT [Fig. 6(a)], the Bragg peaks are quite sharp, while the corresponding ones in the structure factor [Fig. 6(b) taken in the intermediate regime are weaker and vaguer. By comparing Fig. 6 with Fig. 4, one will recognize similarity in the sharpness of Bragg peaks between Figs. 6(a) and 4(a). This fact strongly supports our earlier identification between the FOT in the $\bar{\beta}=2.0\times10^{-3}$ case in Fig. 3 and the BrBoG to BoG melting transition. Therefore, we expect that in the range $1.0\times10^{-4}<p<3.0\times10^{-4}$ in Fig. 2, we have the situation (in the low-T limit) in which the BoG melting is continuous, while the FOT between BrBoG and BoG survives.

Features closely related to those mentioned above are already seen in the $N_L=2$ case. Just like the $\bar{\beta}=2.0\times10^{-3}$ curve of the $N_L=4$ system in Fig. 3, only a single FOT appears in the $N_L=2$ curve in Fig. 5. Through the corresponding data of the structure factor shown in Fig. 7, the single FOT in this $N_L=2$ case is expected to be a remnant of the BrBoG melting which should occur in large N_L limit because the Bragg peaks in Fig. 7(a) are much sharper than those in Fig. 6(b) for $N_L=4$. However, due to the small size parallel to $\mathbf{H}$, the state just above this FOT seems to be not a BoG-like state but the 2D VL. In the context of the 2D quantum case, it implies that at a temperature corresponding to the range $2<N_L<4$, the FOT line between BoG and VL has a critical end point.

Further, we show in Fig. 8 the p dependences of the ΔE curve in the $N_L=2$ case. Again, an increase in p leads even to the disappearance of the remnant of the discontinuous BrBoG melting. By comparing Fig. 2 with Fig. 8, a single FOT corresponding to the BrBoG melting might appear at extremely lower T (i.e., for a larger N_L) when $p=2.0\times10^{-4}$, although no FOT is seen in the $N_L=2$ system, i.e., at higher T.

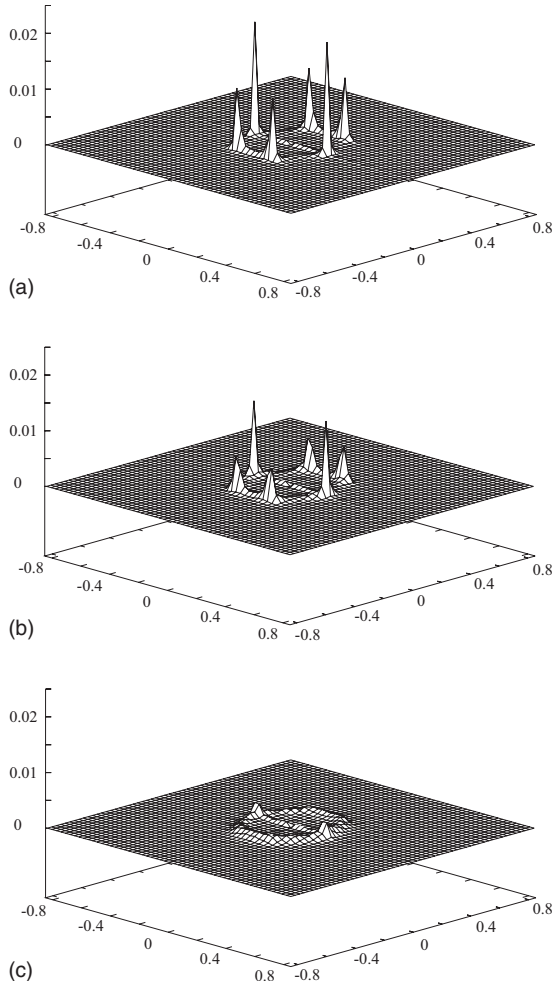

FIG. 6. Snapshots of the structure factor in the $N_L=8$ case in Fig. 5 at different field strengths. (a), (b), and (c) are the results just below the lower FOT ($\alpha=-0.19$), between the two FOTs ($\alpha=-0.15$), and above the higher FOT ($\alpha=-0.11$), respectively. Clearly, the positional order has been completely lost at $\alpha=-0.11$. Similar figures are obtained in the $N_L=4$ case if a different set of α values are chosen.

B. Susceptibility and correlation length

In this subsection, we show results of the susceptibility χ and the glass correlation length ξ_G. Results on these two quantities will become a more firm basis of the existence of FOTs in the quantum 2D case because numerical results of these two quantities are directly comparable with the corresponding theoretical ones[32] in contrast to ΔE. Figure 9 presents the α vs χ data corresponding to the two curves for $p=1.0\times10^{-4}$ and 3.0×10^{-4} of the $N_L=4$ system in Fig. 2. Note that in the context of the thermal 3D case, the field dependence of χ shown here corresponds to the temperature dependence of the specific heat [see the sentences following Eq. (17)]. Near $\alpha=-0.1$, the amplitude fluctuation of Ψ is still active; hence, χ smoothly grows with decreasing α when $\alpha>-0.1$. The fact that χ takes a nearly constant value in the range $-0.15<\alpha<-0.1$ and also near $\alpha\simeq-0.2$ is a consequence of the mean-field result $\chi\bar{\beta}/(L_xL_y)=\beta_A^{-1}\simeq0.86$ for the triangular Abrikosov lattice, where $\beta_A=1.1596$ is the celebrated value of the Abrikosov geometrical factor for the triangular lattice. On the other hand, χ in $p=1.0\times10^{-4}$ deviates from the mean-field value and grows in the range around the value $\alpha\simeq-0.17$ and also in $\alpha<-0.21$, implying precursors of glass transitions. The divergent behavior around the point $\alpha=-0.17$ implies the FOT between BoG and VL, which seems to have been broadened by the finite N_L value. Further, the tendency of χ increasing in $\alpha<-0.2$ with decreasing α is expected to be a reflection of another FOT between BrBoG and BoG lying near $\alpha=-0.235$.

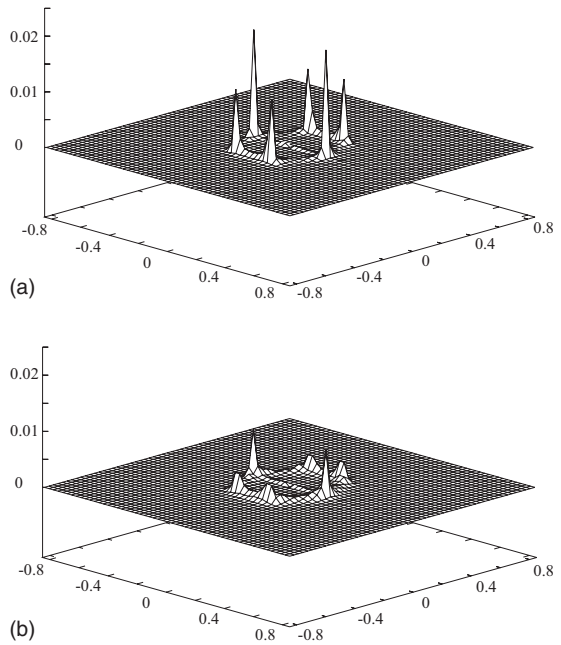

FIG. 7. Snapshots of the structure factor of the $N_L=2$ system for (a) $\alpha=-0.34$ and (b) $\alpha=-0.23$ in Fig. 5. Although quite sharp peaks with hexagonal symmetry appear in (a), such peaks are not visible any longer in (b) just above the transition. Note the α values in these figures which are much lower than the corresponding ones in the $N_L=8$ case.

On the other hand, the χ curve in $p=3.0\times10^{-4}$ does not show a sharp divergence due to the absence of FOT. Never-

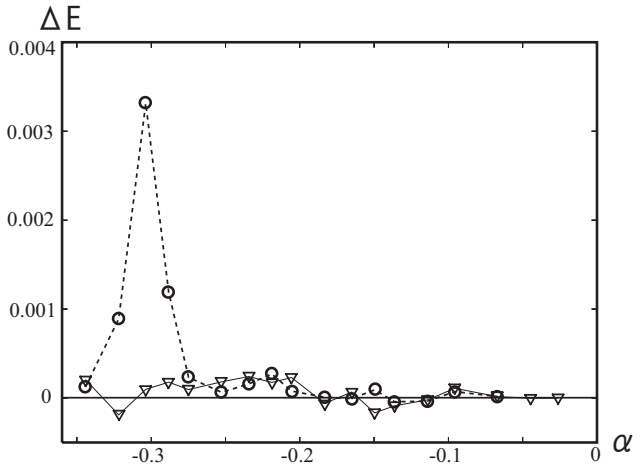

FIG. 8. ΔE data of the $N_L=2$ systems for different pinning strengths, $p=1.0\times10^{-4}$ (open circles) and 2.0×10^{-4} (open triangles). The $p=1.0\times10^{-4}$ result is the same as that in Fig. 5.

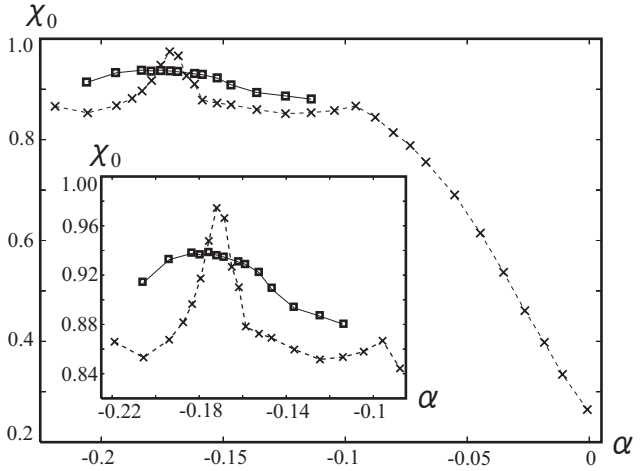

FIG. 9. Results of the *normalized* susceptibility $\chi_0 \equiv \chi\bar{\beta}/L_xL_y$ for $p=1.0\times10^{-4}$ (crosses) and 3.0×10^{-4} (open squares) computed under fixed values $\bar{\beta}=1.0\times10^{-2}$ and $N_L=4$.

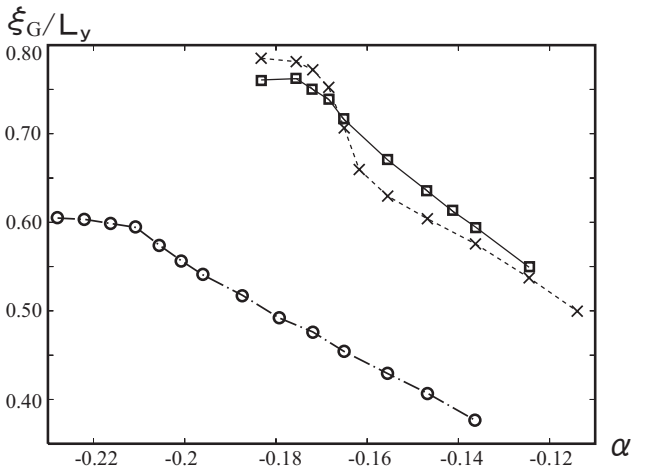

FIG. 10. Results of the dimensionless glass correlation length ξ_G/L_y in the $N_L=2$ and 4 systems. The pinning strength in the $N_L=2$ case (open circles) is $p=1.0\times10^{-4}$, while the curves in the $N_L=4$ case correspond to those in Fig. 9. Note that in the $N_L=4$ case, the correlation length for $p=1.0\times10^{-4}$ becomes longer than that for $p=3.0\times10^{-4}$ below the BoG melting field estimated from the corresponding χ and ΔE data, while the former is shorter than the latter above the melting field.

theless, the plot of χ data in a small α range, shown in the inset of Fig. 9, seems to indicate the presence of a broad cusp or maximum near $\alpha=-0.18$. This might be due to the above-mentioned critical end point, existing in the temperature range corresponding to $2<N_L<4$, of the FOT line between BoG and VL. Alternatively, it may merely reflect the crossover around the *mean-field* 2D glass transition line at $T>0$ and below H_{c2},[23] which, at weak disorder, should lie close to the 2D melting line in the $p=0$ limit. No genuine glass transition occurs along this line in this case; rather this line may be well defined as a sharp crossover line.[37] That is, in this scenario, the broad maximum is due to the *thermal* fluctuation on this crossover line.

The upper two curves in Fig. 10 present data for the glass correlation length ξ_G, normalized by the system size L_y, comparable with the χ curves in Fig. 9. Note that L_y/l is a constant at any α in the present simulations. As the field H decreases from the value $\alpha\simeq-0.12$, ξ_G starts to grow smoothly. This behavior is already seen in Fig. 9 as a gradual growth of χ in the same range. In the presence of the remaining FOT, however, ξ_G rapidly grows around -0.165 and starts to saturate to a finite value near -0.17 because the true BoG phase is not realized in $N_L=4$ systems. On the other hand, in the $p=3.0\times10^{-4}$ case, where the FOTs have been lost, an additional small growth of ξ_G is visible near $\alpha=-0.17$ consistently with the broad maximum of χ in Fig. 9. Note that the saturated value, 0.785, in the $p=1.0\times10^{-4}$ case is larger than the corresponding value 0.76 in the $p=3.0\times10^{-4}$ case. This is consistent with the argument in Ref. 32 that the glass ordering is stronger as the positional correlation of vortices is enhanced. On the other hand, the finite ξ_G value below the higher FOT in the $p=1.0\times10^{-4}$ case is one piece of evidence that a genuine glass phase is not reached at finite temperatures in spite of the presence of FOT accompanied by hysteresis. Further, the fact that ξ_G in $p=3.0\times10^{-4}$ is longer than that in $p=1.0\times10^{-4}$ in the range $-0.16<\alpha<-0.12$ is a consequence of a critical region of the glass fluctuation broadened by, due to the p increase, changing the FOT into a continuous *crossover* on the *mean-field* 2D glass transition line at weak disorder.

On the other hand, ξ_G in the $N_L=2$ case shows a qualitatively similar field dependence to that in the $N_L=4$ and $p=3.0\times10^{-4}$ case except for two features: With increasing $T\propto N_L^{-1}$, ξ_G is clearly lowered, and the field at which the increase in $\xi_G(H)$ starts to saturate is significantly lowered. The latter feature can be regarded as a reflection of the field dependence of the *mean-field* 2D glass transition temperature.

IV. EXPECTED PHASE DIAGRAM AND DISCUSSION

The numerical results shown in Sec. III imply the following parameter dependences of the 2D phase diagram in the quantum regime: First, with increasing defect density proportional to p, the only one FOT line in the $p=0$ case splits into two FOTs while keeping the position of the higher FOT unchanged (see Fig. 1). Thus, with increasing p, BrBoG is destabilized, and the lower FOT (i.e., the melting position of BrBoG) is shifted to a lower field. However, the lower FOT is more robust than the higher one against the disorder, although both of them are lost as p is increased further. Second, as the temperature T is lowered, all glass transition fields increase in general, and the BoG melting, as well as the BrBoG melting, tend to occur as a FOT. Third, with increasing fluctuation strength $\bar{\beta}$, the BoG melting tends to become a FOT, and all glass transitions tend to occur in lower fields. Note that the lowering of T is not equivalent to the reduction in fluctuation. In the present case with quantum fluctuation effects, the cooling leads to the formation of BrBoG, which is the new ordered phase; hence, it also plays a role in effectively *reducing* p. Further, the fact that at a fixed T, the position of BoG to VL transition at weak enough disorder does not deviate from the melting line in clean limit is remarkable and seems to be consistent with the previous experiments.[9,36]

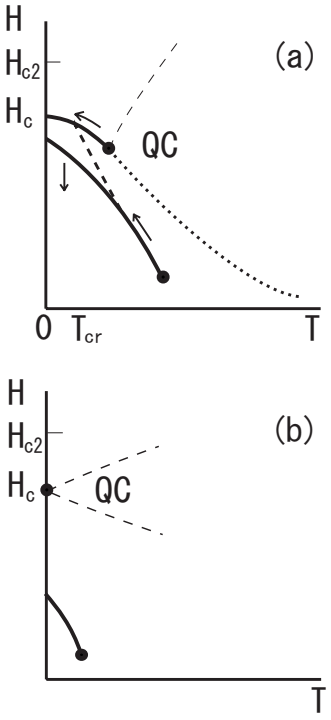

FIG. 11. Expected phase diagrams, focused on the low-T region, of disordered 2D superconductors under magnetic fields perpendicular to the film plane in the cases with (a) low enough p and (b) higher p. In (a), the dotted curve is a crossover line on which the 2D vortex lattice melting in LLL should occur in $p=0$ and, at lower T, is followed by the higher FOT line at weak enough disorder according to the argument in Ref. 10. Each arrow implies an expected change in each line due to an increase in p. Note that the $p=0$ melting field at $T=0$ lies below $H_{c2}(0)$ (Ref. 22). Based on our simulation results, the possibility that, as indicated by a thick dashed curve, the two FOT lines merges at a low but nonzero temperature T_{cr} cannot be excluded. In (b), the critical end point of the higher FOT in (a) reduces to the $T=0$ limit of the dotted curve, although H_c should move to higher fields as p is increased further under a *fixed* $\bar{\beta}$ value (Ref. 38). In both figures, the thin dashed lines indicate boundaries of the QC region due to the critical (end) point of the BoG to VL transition line. According to Eq. (2.15) of Ref. 23, the QC region at fixed T is broadened with decreasing p.

Expected phase diagrams following from these arguments are sketched in Fig. 11. The critical end point of the FOT line between the BoG and VL regimes in Fig. 11(a) may become the origin of a FSI quantum critical behavior reflected as the scaling behavior of resistivity curves. For large enough p, this higher FOT is lost, while the critical end point survives as the quantum critical one. Presumably, the experimental phase diagrams suggested in most of real systems[14,15,17] belong to diagram (b), where the lower FOT may not be present any longer. We believe that, nevertheless, the presence of the lower FOT has been detected in MoGe films[15] with a low p value (see Sec. I). Alternatively, some real materials might have phase diagram (a) if the measurements have been performed at temperatures higher than the end point of the lower FOT in (a). If so, one or two FOTs might be detected in experiments at further lower temperatures.

We should note here that we cannot definitely conclude from our simulation results whether the BoG phase at $T=0$ is present or not. Actually, the size dependences in of the two FOTs shown in Fig. 5 suggest that the intermediate BoG might not occur in the large N_L limit. If so, as indicated by a dashed curve, the two FOT lines in Fig. 11(a) should merge at some temperature T_{cr} very close to $T=0$ so that we might have a single FOT in $0 \leq T \leq T_{cr}$. However, it does not imply that at $T=0$, the BoG phase is always lost in the presence of BrBoG. In fact, under a fixed strength p of the disorder, the changes in vortex states upon decreasing H in the quantum 2D case correspond to those upon cooling in the thermal 3D case, and both of the two glass phases seem to appear in the latter case. In fact, experimental data in YBCO have also shown the presence of two FOTs.[7] Therefore, it is believed that the *generic* phase diagrams in the thermal 3D system and the 2D one at $T=0$, like the solid curves in Fig. 11(a), include *two* FOTs separating the different vortex states below H_{c2}.

In general, model (8) with no dissipative dynamical term is not directly applicable to nongranular amorphouslike SC films in which the dynamics of the SC order parameter is dominated by the Ohmic dissipative term. However, our main conclusion that the FOT between BrBoG and BoG states tends to be more robust than another one between BoG and VL seems to become more reasonable when the dissipative dynamics is incorporated for the following reasons: First, when the dynamics is primarily dissipative, the quantum fluctuation effect is weakened, and then, our results shown in Fig. 3 indicate that the FOT between BoG and VL tends to be lost more easily. In addition, the fact that the Ohmic dissipative term is linear in $|\omega|$ [see Eq. (10)], in contrast to the nondissipative ω^2 term, implies that the positional ordering in BrBoG and, thus, the discontinuous nature of the BrBoG melting will be enhanced further by inclusion of the dissipative term. Therefore, the inclusion of the dissipative dynamical term would lead to a more firm basis for our main conclusion mentioned above, and our identification between the FOT suggested in an experiment[15] and the first-order BrBoG melting transition should be valid irrespective of the details of dynamics of the SC order parameter.

ACKNOWLEDGMENTS

The authors are grateful to T. Nishizaki for showing us his data prior to publication. Numerical computation in this work was carried out using the facilities of the Supercomputer Center, Institute for Solid State Physics, University of Tokyo, and also at YITP in Kyoto University. This work was financially supported by a grant-in-aid from the Ministry of Education, Culture, Sports, Science, and Technology of Japan.

[1] T. Nattermann and A. Scheidl, Adv. Phys. **49**, 607 (2000); T. Nattermann, Phys. Rev. Lett. **64**, 2454 (1990).
[2] T. Giamarchi and P. Le Doussal, Phys. Rev. B **52**, 1242 (1995).
[3] D. S. Fisher, Phys. Rev. Lett. **78**, 1964 (1997).
[4] T. Giamarchi and P. Le Doussal, Phys. Rev. B **55**, 6577 (1997).
[5] D. R. Nelson and V. M. Vinokur, Phys. Rev. B **48**, 13060 (1993).
[6] M. Menghini, Y. Fasano, F. de la Cruz, S. S. Banerjee, Y. Myasoedov, E. Zeldov, C. J. van der Beek, M. Konczykowski, and T. Tamegai, Phys. Rev. Lett. **90**, 147001 (2003).
[7] T. Nishizaki, K. Kasuga, Y. Takahashi, S. Okayasu, and N. Kobayashi, J. Phys.: Conf. Ser. **51**, 267 (2006).
[8] C. J. van der Beek (private communication).
[9] W. K. Kwok, R. J. Olsson, G. Karapetrov, L. M. Paulius, W. G. Moulton, D. J. Hofman, and G. W. Crabtree, Phys. Rev. Lett. **84**, 3706 (2000).
[10] R. Ikeda, J. Phys. Soc. Jpn. **70**, 219 (2001).
[11] C. Dasgupta and O. T. Valls, Phys. Rev. B **72**, 094501 (2005).
[12] S. Koikegami and R. Ikeda, AIP Conf. Proc. **850**, 841 (2006).
[13] T. Nishizaki, K. Shibata, and N. Kobayashi, Physica C **460-462**, 281 (2007).
[14] A. F. Hebard and M. A. Paalanen, Phys. Rev. Lett. **65**, 927 (1990); N. Markovic, C. Christiansen, A. M. Mack, W. H. Huber, and A. M. Goldman, Phys. Rev. B **60**, 4320 (1999).
[15] N. Mason and A. Kapitulnik, Phys. Rev. B **64**, 060504(R) (2001).
[16] M. P. A. Fisher, Phys. Rev. Lett. **65**, 923 (1990).
[17] S. Okuma, T. Terashima, and N. Kokubo, Solid State Commun. **106**, 529 (1998); J. A. Chervenak and J. M. Valles, Jr., Phys. Rev. B **61**, R9245 (2000); V. F. Gantmakher *et al.*, JETP Lett. **71**, 160 (2000).
[18] S. Okuma, K. Suzuki, and N. Kokubo, Physica C **463-465**, 232 (2007).
[19] P. G. de Gennes, *Superconductivity of Metals and Alloys* (Addison-Wesley, Reading, MA, 1989), Sec. 32.
[20] Y. Kato and N. Nagaosa, Phys. Rev. B **48**, 7383 (1993).
[21] J. Hu and A. H. MacDonald, Phys. Rev. B **56**, 2788 (1997). We remark that, in contrast to their argument on the presence of ODLRO, the weak but nonvanishing size dependence of their z shown in Fig. 9 of this reference is consistent with the presence of not off-diagonal long-range order (ODLRO) but quasi-long-ranged phase coherence in the 3D vortex lattice in type-II limit stressed by several authors; [M. A. Moore, *ibid.* **45**, 7336 (1992); R. Ikeda, T. Ohmi, and T. Tsuneto, J. Phys. Soc. Jpn. **61**, 254 (1992)].
[22] R. Ikeda, Int. J. Mod. Phys. B **10**, 601 (1996).
[23] H. Ishida and R. Ikeda, J. Phys. Soc. Jpn. **71**, 254 (2002).
[24] G. Blatter, V. B. Geshkenbein, A. I. Larkin, and H. Nordborg, Phys. Rev. B **54**, 72 (1996).
[25] In two dimensions, the consecutive and continuous melting transitions might be an alternative scenario dependent on microscopic details: S. Doniach and B. A. Huberman, Phys. Rev. Lett. **42**, 1169 (1979); D. S. Fisher, Phys. Rev. B **22**, 1190 (1980).
[26] R. Sasik and D. Stroud, Phys. Rev. B **52**, 3696 (1995).
[27] M. S. Li and T. Nattermann, Phys. Rev. B **67**, 184520 (2003). The Cardy-Ostlund-Carpentier-Le Doussal (COCD) state detected in their thermal 2D simulation is different from the BrBoG regime we argue as the low-field quantum state because the FOT line implying the BrBoG melting disappears with increasing temperature, in contrast to the transition curve in Fig. 10 of this reference. We conjecture that the disorder strengths used in our simulation were strong enough to destroy the COCD state, although the lowest p value we have used cannot be compared directly with their $\tilde{\zeta}_c$.
[28] R. Ikeda, Phys. Rev. B **74**, 054510 (2006); R. Ikeda, J. Phys. Soc. Jpn. **76**, 064709 (2007).
[29] V. N. Popov, *Functional Integrals in Quantum Field Theory and Statistical Physics* (Reidel, Dordrecht, 1983).
[30] R. Ikeda, J. Phys. Soc. Jpn. **69**, 559 (2000).
[31] T. K. Worthington, M. P. A. Fisher, D. A. Huse, J. Toner, A. D. Marwick, T. Zabel, C. A. Feild, and F. Holtzberg, Phys. Rev. B **46**, 11854 (1992).
[32] R. Ikeda, J. Phys. Soc. Jpn. **65**, 3998 (1996).
[33] C. Dasgupta and O. T. Valls, Phys. Rev. B **76**, 184509 (2007), and references therein.
[34] K. Shibata, T. Nishizaki, T. Sasaki, and N. Kobayashi, Phys. Rev. B **66**, 214518 (2002).
[35] Once the spatially varying flux density is included beyond the type-II limit, BrBoG might be unstable. This may be a reason why the BrBoG melting is quite weak and has been rarely detected in the thermal 3D systems. In fact, the second-peak-like line detected in the magnetization measurement (Ref. 7) was not identified in higher fields and may end at a critical point. In contrast, in the quantum 2D case, the assumption of type-II limit is safely valid because of the long λ_L^2/D_t (Ref. 19); hence, BrBoG is expected to be a well-defined phase at $T=0$.
[36] B. Khaykovich, M. Konczykowski, K. Teitelbaum, E. Zeldov, H. Shtrikman, and M. Rappaport, Phys. Rev. B **57**, R14088 (1998).
[37] V. M. Galitski and A. I. Larkin, Phys. Rev. Lett. **87**, 087001 (2001); R. Ikeda, *ibid.* **89**, 109703 (2002).
[38] In real disordered metallic films, an increase in the sheet resistance R_n enhances both $\bar{\beta}$ and p and, consequently, decreases H_c. See R. Ikeda, J. Phys. Soc. Jpn. **72**, 2930 (2003). For the same reason, the R_n dependence of the width of the quantum critical (QC) region will not necessarily coincide with its p dependence indicated in Fig. 11.